Biophysical Chemistry 160 (2012) 1–11

Contents lists available at SciVerse ScienceDirect

Biophysical Chemistry

journal homepage: http://www.elsevier.com/locate/biophyschem

Modeling ADAMTS13-von Willebrand Factor interaction: Implications for oxidative stress-related cardiovascular diseases and type 2A von Willebrand Disease

Nicola Pozzi [a,1], Stefano Lancellotti [b], Raimondo De Cristofaro [b], Vincenzo De Filippis [a,*]

[a] Laboratory of Protein Chemistry, Department of Pharmaceutical Sciences, University of Padua, Padua, Italy
[b] Haemostasis Research Centre, Catholic University School of Medicine, Rome, Italy

HIGHLIGHTS

- The three-dimensional model of ADAMTS13 metalloprotease domain (M13) was built by homology modeling techniques.
- The model was validated against all known artificial and natural mutations found in M13 sequence.
- The peptide vWF(1604-1607) of von Willebrand factor (vWF) was docked into the protease active site.
- The docking model explains why oxidation of Met1606 to methionine sulfoxide inhibits vWF proteolysis by ADAMTS13.
- The model explains why Val1607Asp mutation in type 2A von Willebrand disease accelerates proteolysis of vWF by ADAMTS13.

GRAPHICAL ABSTRACT

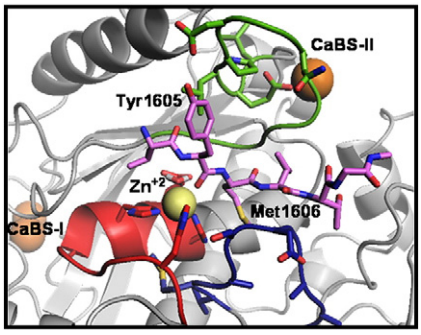

ARTICLE INFO

Article history:
Received 6 May 2011
Received in revised form 26 July 2011
Accepted 27 July 2011
Available online 3 August 2011

Keywords:
ADAMTS13
von Willebrand factor
Oxidative stress
Modeling and docking
Type 2 diabetes
Thrombotic thrombocytopenic purpura

ABSTRACT

The haemostatic potential of von Willebrand factor, a glycoprotein expressed by endothelial cells as ultra-large polymers (UL-vWF)[1], increases with its length, which in turn is regulated proteolytically by ADAMTS13, a zinc-metalloprotease selectively cleaving vWF at the Tyr1605–Met1606 bond. We have recently shown that in vitro oxidation of Met1606, under conditions mimicking those found in diseases characterized by high oxidative stress, severely impairs proteolysis by ADAMTS13, with a resulting pro-thrombotic effect caused by the accumulation of UL-vWF species. Conversely, Val1607Asp mutation, found in vWF from patients with type 2A von Willebrand disease, accelerates proteolysis of vWF, with a final hemorrhagic effect. Considering the physio-pathological importance of ADAMTS13-vWF interaction and the absence of experimental structural data, here we produced by homology modeling techniques a three-dimensional model of ADAMTS13 metalloprotease domain (M13). Thereafter, the vWF(1604–1607) peptide, containing the cleavable Tyr1605–Met1606 bond, was manually docked into the protease active site and the resulting model complex provided us key information for interpreting on structural grounds the variable effects that chemical modifications/mutations in vWF have on proteolysis by ADAMTS13.

Abbreviations: ADAMTS, *A D*isintegrin-like *A*nd *M*etalloprotease with *T*hrombo*S*pondin type I repeats; a.m.u, atomic mass units; CaBS, calcium binding site; M13, the metalloprotease domain of ADAMTS-13; MetSO, methionine sulfoxide; PDB, Protein Data Bank; PN, peroxynitrite; T2DP, type-2 diabetes patients; vWF, von Willebrand factor; VWF-74, the vWF peptide 1596–1669 containing the exchange Cys1669→Ala; UL-vWF, ultra large vWF multimers.

* Corresponding author at: Laboratory of Protein Chemistry, Dept. of Pharmaceutical Sciences, University of Padua, Via F. Marzolo 5, I-35131 Padova, Italy. Tel.: +39 049 827 5698; fax: +39 049 827 5366.
E-mail address: vincenzo.defilippis@unipd.it (V. De Filippis).
[1] Present address: Dept. of Biochemistry and Molecular Biology, Doisy Research Center, SLU, 1cxx100 South Grand Blvd, St. Louis, MO, 63104, USA.

0301-4622/$ – see front matter © 2011 Elsevier B.V. All rights reserved.
doi:10.1016/j.bpc.2011.07.007

1. Introduction

Von Willebrand factor (vWF)[1] is a large (240 kDa; 2050 amino acids) multidomain protein mainly expressed in vascular endothelial cells (EC) and platelets [1]. The majority of mature vWF is stored as ultralarge vWF polymers (UL-vWF, up to 200 monomers with a molecular weight of $20–50\times10^6$ Da) into EC Weibel–Palade bodies or platelets α-granules, from which it is released upon basal and stimulated secretion [2]. Under conditions of normal blood flow, UL-vWF polymers are in a collapsed state and exert only poor haemostatic activity. Conversely, under high shear forces, UL-vWF multimers elongate to unmask A1, A3 and C1 domains, thus initiating primary hemostasis [3,4]. Notably, shorter vWF species are intrinsically less sensitive to shear-induced unfolding [5] and therefore the platelet aggregating potential of vWF is strongly dependent on its length, with longer UL-vWF being more pro-thrombotic than shorter vWF species [6].

The length of UL-vWF is regulated by ADAMTS13 that selectively cleaves vWF at the single peptide bond Tyr1605–Met1606 [7], which is buried in the vWF A2 domain and becomes exposed upon shear-induced unfolding [3]. ADAMTS13, a member of the disintegrin-like and metalloprotease family with thrombospondin type-1 repeats, is a 190 kDa multidomain glycoprotein secreted by the liver in a constitutively active form, with its metalloprotease (M) domain containing three calcium ions and a catalytic zinc in the active site [8,9]. The proposed cleavage mechanism of ADAMTS13, which is common to other matrix metalloproteases, is schematically depicted in Fig. 1. The data accumulated so far indicate that vWF is the only substrate that is cleaved by ADAMTS13 [10]. Hence, the prothrombotic potential of vWF is the result of a dynamic equilibrium between the concentration of bioactive UL-vWF and the proteolytic activity of ADAMTS13. Several genetic, immunological, physical, and chemical factors, affecting both vWF and ADAMTS13, can alter this delicate balance thus promoting either a prothrombotic or hemorrhagic state. For instance, in congenital thrombotic thrombocytopenic purpura (TTP), a life-threatening genetic disease, UL-vWF polymers accumulate as a result of decreased ADAMTS-13 activity, with a resulting thrombotic state [11]. At variance, in type 2A von Willebrand disease (T2A-VWD), a common inherited human bleeding disorder, Val1607Asp mutation induces loss of UL-vWF polymers and hemorrhagic diathesis [12,13].

Peroxynitrite (PN) is produced in vivo by different cell lines (e.g., vascular and intestinal endothelial cells and activated leukocytes) from nitric oxide (•NO) and superoxide ($O_2^{\bullet-}$) radicals, easily crosses membranes and, despite its short biological half-life (~10 ms), it can target biomolecules within 5–20 μm distance from the site of production, inducing cell death by apoptosis or necrosis [14,15]. PN preferentially modifies Cys, Met, Trp, and Tyr to generate sulphenic acid, methionine sulfoxide (MetSO), 2-oxindolylalanine, or 3-nitrotyrosine [16] and its concentration increases (i.e., form $0.3\ \mu M\cdot s^{-1}$ under basal conditions up to $300\ \mu M\cdot s^{-1}$ at inflammatory sites) in pathological settings sustained by oxidative stress and inflammatory processes (e.g., cardiovascular and neurodegenerative diseases, atherosclerosis, rheumatoid arthritis, renal and heart failure, and type 2 diabetes) [14,15]. Very recently, we have shown that treatment of vWF with PN under conditions mimicking those found in vivo attacks the vulnerable Tyr1605–Met1606 bond by oxidizing Met1606 to MetSO, without appreciably modifying Tyr1605 [17,18]. More importantly, oxidation of Met1606 severely inhibits hydrolysis of vWF by ADAMTS13, with a resulting accumulation of the more prothrombotic UL-vWF polymers [17,18]. Hence, we proposed that impairment of ADAMTS13-mediated proteolytic shortening of vWF by Met-oxidation might represent a novel prothrombotic mechanism in the pathogenesis of diseases related to chronic inflammatory states sustained by high oxidative stress and developing at the endothelial level, where also vWF is expressed and released. Consistent with this hypothesis, vWF purified from the plasma of patients with type 2 diabetes (T2DPs), a severe metabolic disease characterized by high oxidative stress and complicated by dramatic thrombotic microagiopathies [19], contains carbonyl levels 5–30 fold higher than those found in vWF from healthy subjects [17]. The carbonyl content is a reliable marker of protein oxidation and in T2DPs it has been found to favorably correlate with a greater proportion of UL-vWF polymers [17].

Considering the importance of ADAMTS13 in hemostasis and the pathological implications of PN-induced vWF oxidation, in the absence of any experimentally determined three-dimensional structure of the enzyme, here we first produced a homology model of ADAMTS13 metalloprotease domain (M13) and then modeled ADAMTS13-vWF interaction by manually docking the cleavable vWF segment ^{1604}*Val-Tyr-Met-Val*^{1607} into the protease binding cleft. The docking model allowed us to explain the variable and even opposing effect that vWF modifications (i.e., Met1606 → MetSO, or Val1607 → Asp) have on the efficiency of ADAMTS13 hydrolysis.

2. Methods

2.1. Model building

Homology modeling and energy calculations were performed using the Molecular Operating Environment (MOE) suite, version 2008.10 (The Chemical Computing Group, Montreal, Canada). The sequence ^{76}Ala-Ser^{373}, encompassing the putative metalloprotease (M) (^{76}Ala-Pro^{286}) and disintegrin-like (D) (^{287}Arg-Ser^{373}) domain of ADAMTS13 (MD13), was collected from the SwissProt protein sequence database (entry code: Q76LX8) and a sequence similarity search for the polypeptide chain against all other sequences in the data base was

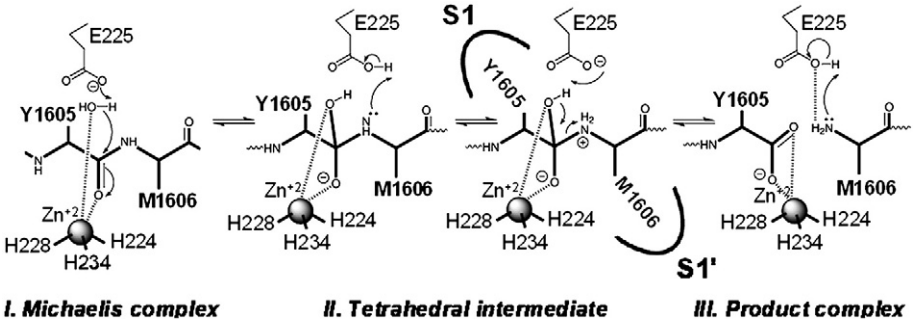

Fig. 1. Proposed mechanism of ADAMTS13 catalysis [55]. Substrate binding occurs in an extended conformation, with Tyr1605 interacting with the protease S1 site and Met1606 with the S1′ site, to form the Michaelis complex (step I). In this complex, the catalytic zinc ion, represented as a sphere, is coordinated in a pentameric fashion by the Nε2 atoms of the three conserved histidines, by the carbonyl group of Tyr1605 at the scissile bond and by a catalytic solvent molecule, which is strongly polarized by the zinc ion and the carboxylate group of Glu225. In the Michaelis complex, the polarized water is highly nucleophilic and attacks the carbonyl group to form a tetrahedral intermediate (step II), which undergoes two consecutive proton shuffling reactions and evolves into the cleavage products with the formation of new carboxylate and α-ammonium groups (step III).

performed using the "PDB-Search" option. Hence, the crystallographic structure of ADAMTS4 MD domains (MD4),[2] solved at 2.8-Å resolution in the inhibitor-bound (2rpj_A) form [20], was used as a template for modeling MD13 by homology. Alternatively, the ADAMTS13 sequence ^{76}Ala-Asp^{284} was modeled on the M-domain structure of ADAMTS5, M5 (3b8z_A; sequence ^{264}Ser-Asp^{474}), solved at 1.4-Å resolution in the inhibitor-bound form [21]. Sequence alignment was performed using the "Align" tool, based on the BLOSUM62 substitution matrix, with increased values for the gap start penalty of 7 and gap extension penalty of 1. Thereafter, the model was built using the automated "Homology Model" tool comprising the following steps: 1) initial partial geometry specification, whereby a partial geometry for the target sequence was copied from regions of the template structure; 2) modeling of outgaps, insertions and deletions starting from fragments of high resolution structures in the PDB; 3) creation of independent protein models using a side-chain rotamer library and loop dictionary derived from known X-ray structures in the PDB; 4) selection of the best model candidate according to the GB/VI scoring function; 5) refinement of the model using the AMBER-99 force field as implemented in MOE; 6) evaluation of the stereochemical quality of the model by the "Quality Evaluation" tool in MOE or the WhatCheck [22] and ProCheck [23] software programs. The atomic coordinates of MD13 and M13 were subjected to several cycles of restrained energy refinement, using the AMBER-99 force field [24], in order to compensate for unfavorable intramolecular contacts introduced during modeling. A 1000-steps descent gradient was performed, followed by a conjugate gradient minimization until the r.m.s. of the potential energy was less than 0.1 kcal $mol^{-1}\cdot Å^{-1}$. Satisfactory stereochemistry for the Ca^{+2} binding sites in M-13 model was obtained by copying the coordinates of Ca^{+2}-ions of the M-5 template (3b8z) and imposing in the M13 model the Ca^{+2}-ligand distances of the template structure. In the final step, local restrained energy minimization was performed. A similar procedure was used for modeling the disulfide bond Cys242–Cys265, which was not formed after building M13 model. The Sγ–Sγ distance was constrained at 2.04 Å, typical of S–S bonds in proteins, and then local restrained energy minimization was performed.

Amino acid substitutions in M13 (Table 1) were simulated with the Mutate option in MOE. Side chain conformation was modeled using the Rotamer Explorer option, followed by local restrained minimization within 5-Å radius from the Cα atom of the mutated residue. Thereafter, the relative conformational stability of each M13 mutant was estimated by a resident version of the Fold-X 3.0 program [25], using default parameters, without taking into account water molecules.

2.2. Docking

The peptide segment ^{1604}*Val-Tyr-Met-Val*^{1607} of vWF, vWF(1604–1607), comprising the cleavable ^{1605}Tyr–Met^{1606} bond, was manually docked into the binding cleft of M13 model. As a starting template for ligand modeling, we used the crystallographic structure of the matrix metalloproteinase 12 (MMP12) (PDB code: 2oxz; 1.9-Å resolution) [26], obtained by soaking the MMP12 crystal with the peptide segment ^{204}*Pro-Gln-Gly-Ile-Ala-Gly*^{209} of the α1 collagen chain. This peptide is known to be cleaved by MMP12 at the *Gly–Ile* bond, where *Gly*^{206} and *Ile*^{207} represent the P1 and P1′ specificity sites of the substrate for the protease, respectively. Of note, only the cleavage products ^{205}*Gln-Gly*^{206} and ^{207}*Ile-Ala-Gly*^{209} could be detected in the crystal structure. The choice of MMP12-collagen complex was motivated by the following considerations: 1) MMP12 has protein fold, active site geometry, substrate binding mode, and catalytic mechanism similar to that of the M domains of ADAMTS4 and ADAMTS5 we used for modeling M13 structure; 2) as shown in Fig. S3, the active-site geometry of MMP12 is superimposable with that of the modeled M13; 3) to the best of our knowledge, 2oxz.pdb is the only available structure of a metzincin protease noncovalently bound to a peptidyl substrate either at the primed and nonprimed side of the scissile bond. The geometry of ^{205}*Gln-Gly*^{206} segment bound to MMP12, therefore, stores key information (e.g., distance and orientation of the carbonyl oxygen from the zinc ion and the conserved catalytic water molecule) for modeling the vWF sequence ^{1604}*Val-Tyr-Met-Val*^{1607} into the active site cleft of M13. The backbone geometry of *Gln-Gly* dipeptide was first copied from the template structure of MMP12 to the M13 model and then elongated toward the C-terminus in an extended conformation ($\phi = -120°$; $\psi = +140°$). After side-chain substitution, the backbone structure (i.e., Cα(Tyr^{1605})-CO(Tyr^{1605})-NH(Met^{1606})-Cα(Met^{1606})) of the scissile bond was constrained in the conformation assumed by the C-terminal carboxylate of *Gly*^{206}, whereas either ligand and receptor atoms within 8-Å distance from the scissile bond were energy minimized using

Table 1
Effect of mutations, found in ADAMTS13 gene of TTP patients, on the proteolytic activity of ADAMTS13.

Gene mutation	Amino acid exchange	Clinical manifestations of TTP[a]	Proteolytic activity[b]	Method used for estimating ADAMTS-13 activity [c,d]	Reference
c.237C>G	I79M	?[e]	?[e]	Plasma[c]	[34]
c.262G>A	V88M	Moderate	18%	In vitro expr[d]	[35,36]
			40%	in vitro expr	
c.286C>G	H96D	Severe	2–7%	Plasma	[37]
c.304C>T	R102C	Severe	2–7%	Plasma	[37]
c.356C>T	S119F	Moderate	50–60%	Plasma	[38,39]
			50%	in vitro expr	
c.533T>C	I178T	Severe	0.5–3%	Plasma	[40]
c.577C>T	R193W	Severe	~0%	In vitro expr	[41]
c.587C>T	T196I	Severe	2–7%	Plasma	[37]
c.607T>C	S203P	Severe	<5%	Plasma	[34,42]
			~0%	in vitro expr	
c.695T>A	L232Q	Severe	2–6%	Plasma	[43]
c.702C>A	H234Q	Severe	<3%	Plasma	[44]
c.703G>C	D235H	Mild	n.a.[f]	n.a.[f]	[45]
c.749C>T	A250V	Severe	~0%	In vitro expr	[46]
c.788C>G	S263C	Mild	37%	Plasma	[43]
c.803G>C	R268P	Severe	~0%	In vitro expr	[47,42]
				in vitro expr	

[a] The clinical manifestations in TTP patients were classified as severe, moderate and mild, according to the disease symptoms reported [11].
[b] The proteolytic activity of ADAMTS13 is reported as the per cent ADAMTS13 activity of plasma from normal individuals (100%) or of wild-type recombinant ADAMTS13.
[c] The activity of ADAMTS13 was determined in the plasma of TTP patients without any further purification.
[d] ADAMTS13 mutants were expressed in eukaryotic systems in vitro, purified and tested for proteolytic activity.
[e] Mutation I79M occurs in a compound heterozygote containing also the deleterious mutation R268P.
[f] Data not available.

AMBER-99 force field and the LigX tool in MOE. To better refine the docked complex, a rotamer exploration of all side chains directly (within 5-Å distance) involved in the binding was carried out using the "Rotamer Search" tool, while energy minimization was run until the conjugate r.m.s. gradient was less than 0.05 kcal/(mol·Å). The geometry of MetSO in the M13-vWF(1604–1607)/Met1606MetSO complex was optimized using the bond length and angle parameters derived from the crystal structure of the corresponding free amino acid [27].

3. Results and discussion

3.1. Modeling ADAMTS13 metalloprotease (M) and disintegrin (D) domains

After sequence alignment, the best score was obtained for the aggrecan-cleaving proteases ADAMTS4 ($E = 4.3 \times 10^{-33}$) and ADAMTS5 ($E = 2.5 \times 10^{-33}$) and for the anti-angiogenic protease ADAMTS1 ($E = 2.5 \times 10^{-21}$) (see Fig. 2). The chain ^{76}Ala-Ser^{373},

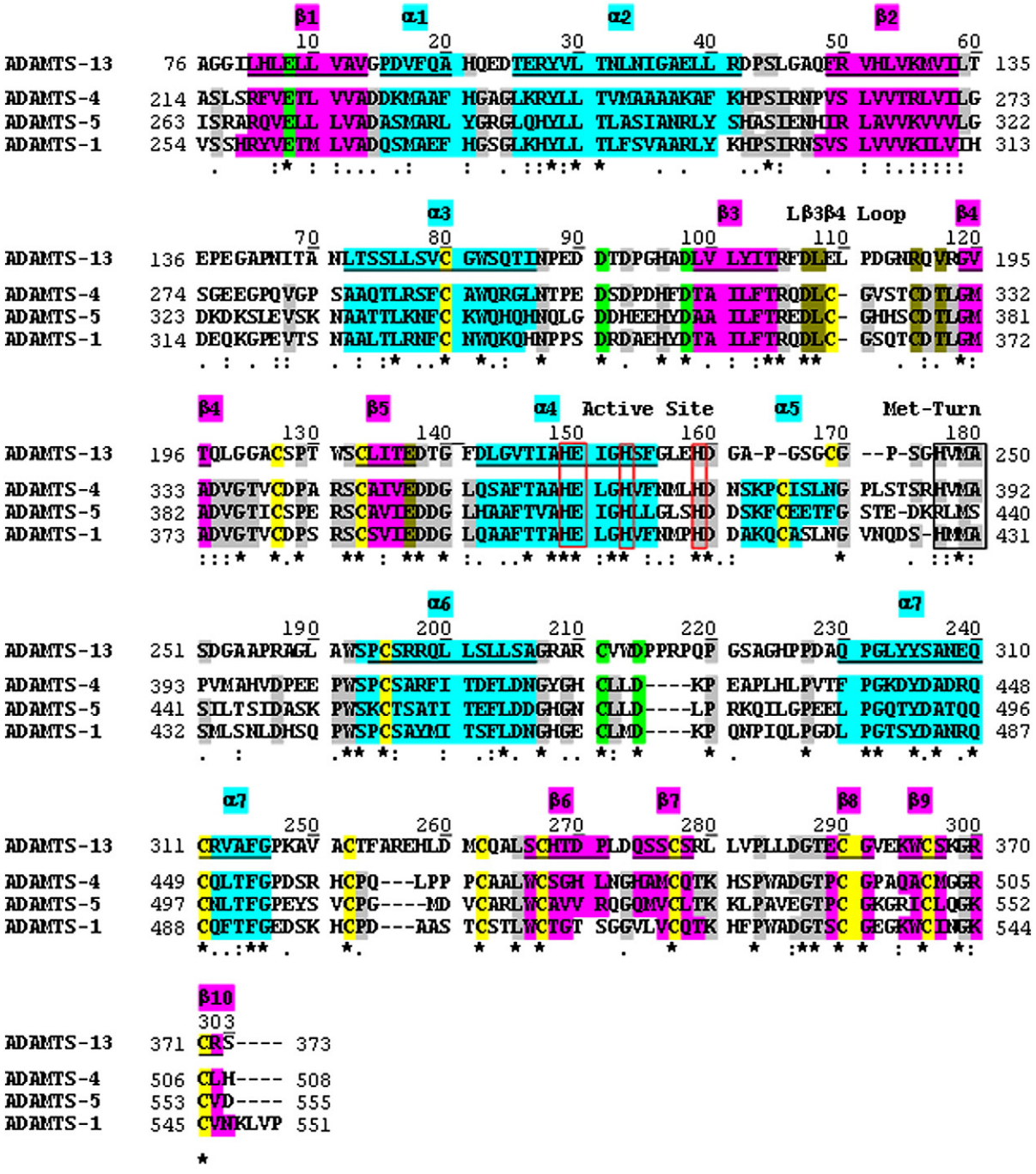

Fig. 2. Structure-based alignment of ADAMTS13 with ADAMTS-1, -4, and -5. The alignment was carried out using the "Align" tool in MOE. The symbols under the aligned sequences indicate identity (*), or high (:) and low (.) similarity of the amino acids, according to their physico-chemical properties. Helical segments are colored in cyan, while β-strands are in magenta. For ADAMTS13, the predicted secondary structure segments are underlined. Highly conserved residues located outside the helical or β-sheet structures are colored in gray, while Cys-residues are in yellow. The amino acids forming the CaBS-I are colored in light green, while those in the CaBS-II are in dark green. The Zn^{+2}-chelating amino acids in the active site are boxed in red, while those forming the "Met-turn" are boxed in black. Sequence and secondary structure elements were deduced from the SwissProt and Protein Data Bank. ADAMTS1: Q9UHI8, 2jih_A. ADAMTS4: O75173, 2rjp_A. ADAMTS5: Q9UNA0, 3b8z_A. ADAMTS13: Q76LX8. Of note, the peptide segment comprising α5-helix, in ADAMTS13 is predicted to assume a nonregular conformation.

encompassing the M and D domains of ADAMTS13 (MD13), was then modeled on the low-resolution (i.e., 2.8 Å) structure of MD4, (2rpj_A) [20] (Fig. S1). MD13 sequence ^{76}Ala-Ser^{373} displayed 32.5% sequence identity with MD4 sequence ^{214}Ala-His^{508}. However, a better stereochemistry was obtained when the ^{76}Ala-Asp^{284} chain, encompassing the M13 domain, was modeled on the structure of ADAMTS5 metalloprotease domain (M5) (3b8z_A) [21], solved at 1.4-Å resolution (Fig. 3). M13 sequence ^{76}Ala-Asp^{284} displayed 26.8% sequence identity and 38.3% sequence similarity with M5 sequence ^{264}Ser-Asp^{474}. The structural organization of M13 resembles the α/β structure typical of the metzincins family, with a shallow active-site cleft located at the interface between a major "upper" domain and a small "lower" domain (Fig. 3A) [28,29]. The modeled structures can be easily superimposed to those of MD4 or M5 templates, showing variability only in the peripheral loop regions (Fig. S1). Significant differences exist in the Lβ3β4-loop, where a disulfide bond is missing in ADAMTS13, and in the peptide segment downstream of α4-helix, which assumes a non-regular conformation in M13 whereas it is helical in other ADAMTS structures (Fig. 2 and Fig. S1). Evaluation of the stereochemical quality of the models reveals that essentially no clash is present in the model structures and that most of the amino acids occupy low-energy side-chain and backbone conformations, as shown in Fig. S2 (Supplementary Materials).

In the M13 sequence the zinc-binding consensus motif of metzincins family (HEXXHXXGXXH) is totally conserved (Fig. 2) and the catalytic zinc ion is tetrahedrically coordinated by the Nε2 atoms of the three His-residues and by a catalytic water molecule, which is polarized by Glu225 and is involved in the nucleophilic attack at the scissile bond of the peptide substrate (Fig. 3B) [28,29]. The chain then continues with the Met-turn (His247–Ala250), containing an absolutely conserved methionine (Fig. 2) at position 3 that forms a hydrophobic base beneath the catalytic Zn^{+2} and is responsible for the structural integrity of the zinc-binding site in metzincins [30]. As shown in Fig. S1, downstream of α6-helix the chain wraps around the back of the M domain and then returns to the front side to form the smaller disintegrin-like D domain (i.e., sequence ^{299}Ala-Ser^{373}), which seems to restrict accessibility to the S1′ site. The D domain has a unique fold of two consecutive α-helices and two short β-sheets (Fig. S1C) stabilized by four conserved disulfide bonds (see Fig. 2). Notably, the modeled D13 structure is largely superimposable to that of the corresponding D domain in the crystallographic structure of the non-catalytic ADAMTS13 domains (3ghm.pdb) [31], except for the ^{340}Asp-Leu^{350} region. Excluding the latter segment, the rmsd value drops from 1.0 to 0.7 Å.

From the conservation of the Cys-residues in ADAMTS family (Fig. 2) and in the absence of direct chemical determination of disulfide connectivities in M13, it can be predicted that three of the four disulfide bonds present in the three-dimensional structure of M1, M4, and M5 are also formed in M13 (Fig. 3A), whereas the S–S bond in the Lβ3β4 loop is missing, as already observed in ADAMTS-2, -3 and -14. In our model, the disulfide Cys155–Cys208 connects α3-helix to β5-strand in the central β-sheet, while Cys242–Cys265 in the "lower" domain helps to stabilize the active site and the "Met-turn". Finally, the third disulfide Cys202–Cys281 links the Lβ4β5 loop to the chain segment connecting the M and D domains, thus strengthening the interactions between the "upper" and "lower" domain.

The structure-based alignment of M13 with other members of ADAMTS family shows that most of the amino acids involved in the CaBSs of M1, M4 and M5 are also conserved in M13. Hence, two putative calcium binding sites, CaBS-I and CaBS-II, can be identified in M13 (Fig. 3C,D). Our model (Fig. 3C) shows that CaBS-I can accommodate two Ca^{+2} ions and is formed by highly conserved

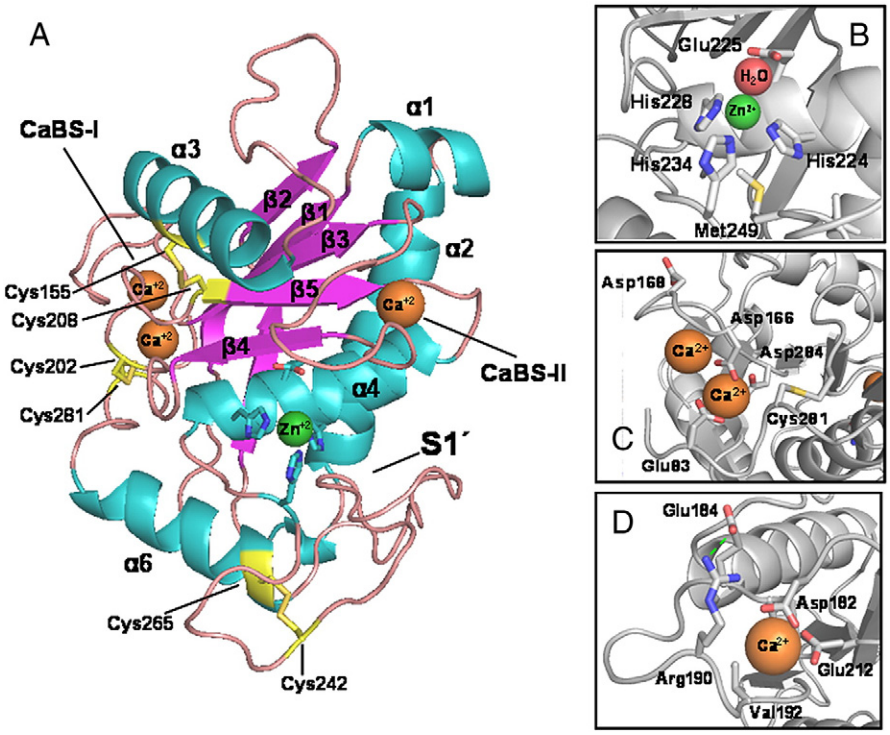

Fig. 3. (A) Structural organization of ADAMTS13 metalloprotease domain (M13). The model was obtained by homology on the M5 structure (3b8z_A). β-strands are colored magenta, helices are in cyan, and disulfide bridges are yellow; the catalytic zinc (green) and the calcium ions (orange) are also shown. (B–D) Close-up view of the catalytic and calcium binding sites. (B) The Zn^{+2}-binding motif is structurally conserved and the catalytic zinc ion is tetrahedrically coordinated by His224, His228 and His234, and by a catalytic water molecule that is polarized by Glu225 for nucleophilic attack. (C) CaBS-I is contributed by the carboxylates of Glu83 (β1-strand), Asp166 and Asp173 (Lα3β3 loop), and Asp284 (connector loop), and by the carbonyl oxygen-atoms of Asp166 (Lα3β3 loop) and Cys281 (connector loop). (D) CaBS-II is contributed by the carboxylates of Asp182 and the carbonyl oxygen-atoms of Leu183, Arg190 and Val192 in the Lβ3β4 loop, and by the carboxylate of Glu212 in the β5-strand. The salt bridge possibly forming between Glu184 and Arg190 is indicated by a dashed line (green). Ribbon drawing was generated using the program PyMol (DeLano Scientific LLC, CA).

amino acids in the Lα3β3 loop, the β1-strand, and the connector loop downstream of α6-helix (Fig. 2). At variance with CaBS-I, CaBS-II is adjacent to the active site and binds a single Ca^{+2} ion (Fig. 3D). It is contributed by Asp182, Leu183, Arg190 and Val192 in the Lβ3β4 loop, and by Glu212 in the β5-strand. Of these, only Asp182, Leu183 and Glu212 are conserved in ADAMTS family (Fig. 2). As already mentioned, the disulfide bond that in other ADAMTS cross-links the Lβ3β4 loop, is missing in ADAMTS13. Nevertheless, the two bridged cysteines are replaced by Glu184 and Arg190, which in our model form a salt-bridge and thus may help to stabilize the Lβ3β4 loop and CaBS-II (Fig. 3D).

3.2. Validation of M13 model by experimental data

Our model was successfully validated against the effect that all known artificial and natural mutations in the M13 sequence have on the proteolytic activity of ADAMTS13. In particular, artificial mutations are localized in the calcium-binding site II [32,33] (Figs. 4 and 5), whereas natural mutations are distributed throughout the metalloprotease domain (Table 1 and Figs. 4 and 6) causing mild to severe symptoms of congenital thrombotic thrombocytopenic purpura (TTP), a genetic disease characterized by reduced proteolytic activity of ADAMTS13 and accumulation of UL-vWF species [11]. Finally, the effect of mutations on the energetics of M13 mutants was estimated using the Fold-X force field (Fig. 7) and correlated with the severity of clinical manifestation of TTP.

3.2.1. Artificial mutations in M13 calcium-binding sites (CABSs)

Our model is consistent with recent biochemical and mutagenesis studies indicating that ADAMTS-13 contains two calcium binding sites, CaBS-I and CaBS-II [32,33]. In particular, CaBS-I is a low-affinity site, contains two Ca^{+2} ions and mainly exerts a structural role; CaBS-II, instead, binds only one Ca^{+2} ion, has high affinity for calcium and plays a functional role, likely by opening the S1/S1′ sites for substrate binding [32]. The model also shows that (at variance with CaBS-I) CaBS-II is stabilized by a network of ionic interactions within the Lβ3β4 loop or between this loop and nearby regions of the enzyme. These interactions help to stabilize the Lβ3β4 loop and orient the side-chains of the chelating amino acids in the right conformation for calcium binding. Single-point mutations of selected amino acids with Ala in CaBS-II indicate that: 1) mutation of Asp187, Arg190, Arg193 or Glu212 markedly decreases Ca^{+2} binding affinity and protease activity by 2–10 fold; 2) Glu184Ala exchange, instead, only moderately reduces the affinity for calcium and does not appreciably affect ADAMTS-13 function [32,33]. As discussed in the following, our model provides convincing structural interpretation of these results (Fig. 5).

Asp187Ala The carboxylate of Asp187 in the Lβ3β4 loop, shaping the S1 site, is hydrogen bonded to Asn146 and Thr148 in the N-terminal region of α3-helix, thus contributing to stabilize the S1 site. Therefore, disruption of these hydrogen bonds by Ala-mutation is expected to decrease Ca^{+2} affinity and thus optimal proteolytic function (Fig. 5A).

Glu212Ala Glu212 is directly involved in Ca^{+2} binding and therefore the mutation of this residue with Ala can be easily predicted to alter both protease structure and function (Fig. 5B).

Arg190Ala Arg190 forms a salt bridge with Glu184, thus helping to stabilize the Lβ3β4 loop, shaping CaBS-II. Furthermore, Arg190 is also

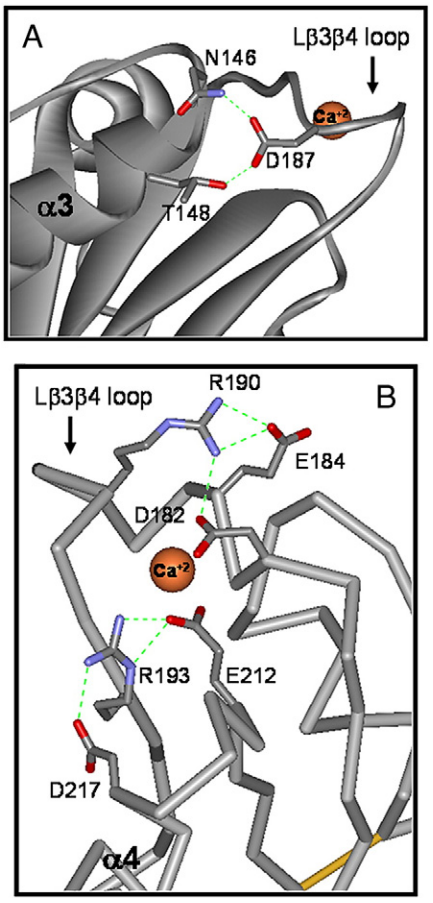

Fig. 5. M13 model: close-up view of the hydrogen bond network involving Asp187 (A) and ionic interactions in CaBS-II (B). Hydrogen bonds are indicated by dashed lines (green), while calcium ions and disulfides are in orange and yellow, respectively.

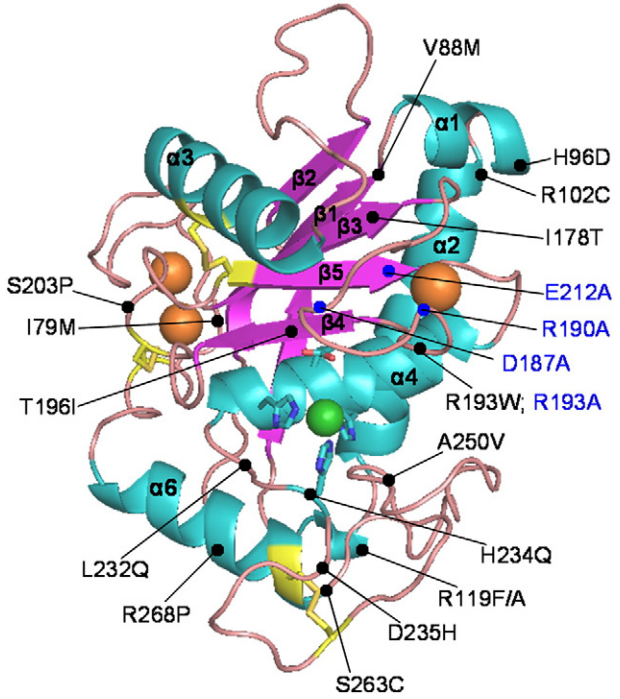

Fig. 4. Artificial (blue labeled) and natural (black labeled) mutations in ADAMTS-13 metalloprotease domain. The effect of natural mutations in ADAMTS13 gene are reported in Table 1. Helical and β-sheet secondary structures are colored in cyan and magenta, respectively. Disulfide bridges are in yellow, while calcium and zinc ions are in orange and green, respectively. The side chains of the catalytic His224, His228, His234 and Glu225 are also shown.

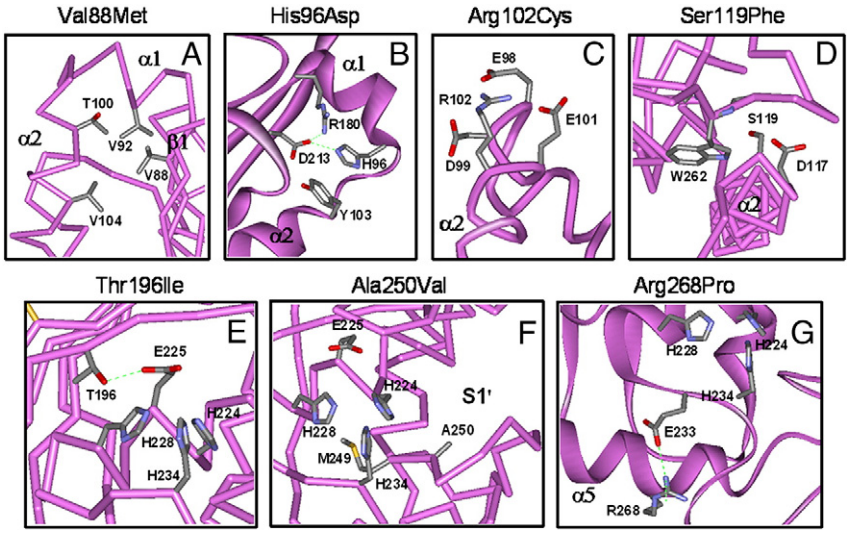

Fig. 6. M13 model: close-up view of the chemical environment surrounding selected amino acids that are mutated in ADAMTS13 gene of TTP patients.

electrostatically coupled to Asp182 in the coordination shell of Ca^{+2}. Hence, Arg → Ala exchange can be safely predicted to destabilize the Lβ3β4 loop, with a resulting decrease of Ca^{+2} affinity and proteolytic activity. Our model also reasonably explains why Glu184Ala mutation reduces calcium affinity by only 3-fold and does not appreciably affect ADAMTS-13 function [32,33]. In fact, the lack of Glu184 disrupts the surface exposed salt bridge Glu184–Arg190, but does not impair the possibility for Arg190 to favorably interact with Asp182 in the coordination shell, without altering the conformation of CaBS-II (Fig. 5B).

Arg193Ala Arg193 is salt bridged to Glu212 in the coordination shell of Ca^{+2} and to Asp217 in the N-terminal region of α4-helix, containing the catalytic amino acids His224, Glu225 and His228. Therefore, Arg193Ala exchange is expected to destabilize the electrostatic link connecting CaBS-II to the active site, thus explaining the lower proteolytic efficiency of the mutant enzyme [33] (Fig. 5B).

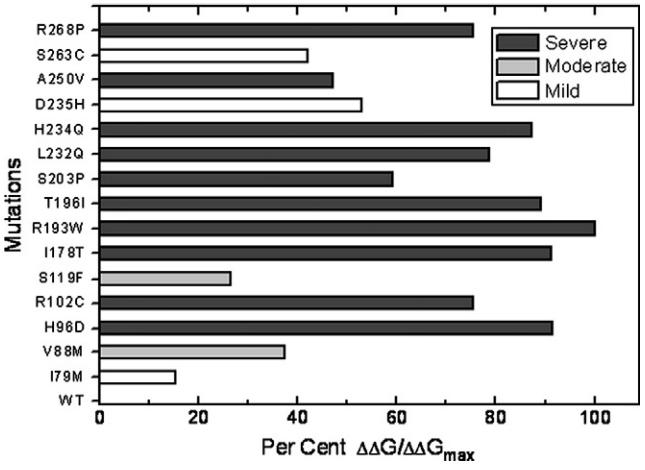

Fig. 7. Relative stability of M13 mutants calculated with the Fold-X force field. The conformational stability of each mutant ($\Delta\Delta G = \Delta G^{M} - \Delta G^{WT}$) is expressed as the per cent variation with respect to $\Delta\Delta G_{max}$, calculated for the R193W mutant. Mutations causing mild, moderate, or severe clinical manifestations of TTP are shown in white, light gray and dark gray, respectively. A positive value of $\Delta\Delta G/\Delta\Delta G_{max}$ indicates destabilization induced by mutation. For the R102C mutant, where the mutated amino acid is at the interface between the M and D domain, calculations were carried out on the modeled MD13 structure.

3.2.2. Natural pathogenic mutations of M13

Ile79Met Based on the reduced ADAMTS-13 activity of plasma from selected TTP patients, this mutation has been proposed as causative of the disease [34]. From our model, however, Ile79Met mutation does not seem to have dramatic consequences neither on the enzyme structure nor function. Ile79 is, in fact, located in the N-terminal region of the metalloprotease domain, on the protein surface and quite distant from the active site. Notably, this mutation has been found in association with the Arg268Pro mutation, which is well known to abolish protease activity by itself (Table 1) [42,47]. In this view, the hypothetical modest effect of Ile79Met mutation would be masked by the deleterious effect of Arg268Pro mutation (Fig. 4).

Val88Met Val88 is located at the C-terminal end of β1-strand, at about 20 Å distance from the catalytic site, and buried in the protein core. Modeling Val → Met exchange suggests that it is difficult, if not impossible, to accommodate Met without severe clashes. In fact, the longer Met side-chain clashes against Val92 in α1-helix or Thr100 and Val104 in α2-helix, which is tightly packed with the "catalytic" α4-helix and the Lα4α5 loop, shaping the S1′ site. Hence, the perturbation introduced by Val → Met exchange might be transmitted long-range to the active site, with a moderate decrease of catalytic function [35,36] (Fig. 6A).

His96Asp His96 is located at the C-terminal end of α1-helix; it is hydrogen bonded to Asp213 in the Lβ5α4 loop and stacked onto the aromatic ring of Tyr103 in α2-helix, which also makes a hydrogen bond with Asp213. Hence His96Asp mutation is expected to affect M13 structure and severely decrease function [37] by 1) introducing a strong electrostatic repulsion with Asp213 that may alter the correct packing of α2 and α4 helices, 2) destroying the energetically favorable His96–Tyr103 aromatic–aromatic interaction [48], and 3) introducing an unfavorable charge–helix dipole interaction [49] (Fig. 6B).

Arg102Cys Arg102 is located at the N-terminal region of α2-helix, facing the D domain. Arg102 in the native M13 structure stabilizes a negative cluster formed by Glu101, Asp99, and Glu98. Therefore, replacement of a positive amino acid like Arg with a neutral amino acid like Cys is expected to strongly destabilize M13 and to possibly weaken the interactions between the M and D domains, with a resulting decrease of proteolytic function [37] (Fig. 6C).

Ser119Phe and Ser119Ala Our model suggests that the –OH group of Ser119 in the Lα2β2 loop makes two hydrogen bonds with the amide –NH group of Trp262 in the Lα4α5 loop and with the

carboxylate of Asp117 at the C-terminal end of α2-helix. Trp262 is absolutely conserved in ADAMTS family (see Fig. 2) and forms a hydrophobic floor at the bottom of the S1′ site. Hydrogen bonding of Ser119 with Asp117 locally stabilizes the protein structure by alleviating unfavorable charge–helix dipole interaction [49]. The loss of these hydrogen bonds might alter the local conformation of the S1′ site with a resulting moderate decrease of protease activity [38,39]. That alteration of hydrogen bonding is the major cause of the deleterious effect of Ser119Phe mutation is also supported by the fact that the side-chain of Phe can be modeled without major clashes and, more importantly, by the reduced proteolytic activity of the artificial Ser119Ala mutant [39] (Fig. 6D).

Ile178Thr Ile178 is located in the β3-strand, behind the catalytic α4-helix, in a highly apolar environment formed by Val88 (β1-strand), Val104 (α2-helix), Lue176 (β3-strand), and Leu218 (α4-helix). The replacement of Ile with a more polar and smaller residue like Thr destabilizes the native M13 structure, and thus strongly decreases protease function [40], not only by weakening hydrophobic interactions, but also by creating an uncompensated cavity that may alter the precise side-chain packing in a "hot" region nearby the catalytic site (Fig. 4).

Arg193Trp At variance with the artificial Arg193Ala mutation, that was found to reduce ADAMTS13 activity by only 4-fold [33], Arg → Trp exchange completely abolished enzyme activity [41]. As for Agr193Ala, Arg193Trp exchange disrupts ionic interactions that Arg193 counteracts in CaBS-II. In addition, the bulky Trp side-chain further alters side-chain packing in CaBS-II, enhances the hydrophobic surface that becomes exposed to the solvent, and (partially) occludes entrance of the S1′ site (Fig. 5B).

Thr196Ile Our model suggests that Thr196 side-chain in the β4-strand may help, via hydrogen bonding, to correctly position Glu225 for catalysis. Upon Thr196Ile mutation, this interaction is lost and the Cδ1 methyl of Ile clashes against the backbone carbonyl oxygen of the catalytic Glu225 and the imidazole ring of the catalytic His228. These changes are expected to alter the stereochemistry of the catalytic site in ADAMTS13, thus explaining the strong decrease of proteolytic function [37] (Fig. 6E).

Ser203Pro Ser203 is solvent exposed in the Lβ4β5 loop, precedes the conserved Pro204 and follows the conserved disulfide bridge Cys202–Cys281 connecting the "upper" and "lower" domains (Fig. 3). The presence of a sterically constrained –Pro-Pro- sequence is likely to perturb the conformation of Lβ4β5 loop and impair correct positioning of the disulfide bond Cys202–Cys281 and α6-helix lying beneath the catalytic site. The backbone geometry of Ser203 in our model structure (ϕ: −156°, ψ: +71°) is indeed not compatible with the preferred conformation of Pro, with ψ centered at +145° [49]. Hence, it is conceivable that local perturbations introduced by Ser → Pro mutation can be transmitted long-range to the active site with a resulting deleterious effect on ADAMTS13 function [34,42] (Fig. 4).

Leu232Gln Leu232 follows the catalytic α4-helix between His228 and His234, is adjacent to the active site and is buried in a hydrophobic environment formed by Phe230 (α4-helix) and the conserved Met249 (Met-turn) and Trp262 (Lα4α6 loop). In other ADAMTS family members, the position equivalent to Leu232 is always an apolar amino acid (i.e., Leu, Ile, or Met). The strong decrease of enzymatic activity of the Leu232Gln mutant [43] can be explained considering that replacement of Leu with the longer and more polar Gln may alter the hydrophobic packing in a key region for catalysis (Fig. 4).

His234Gln His234 chelates the catalytic zinc ion and is highly conserved throughout the metzincin family. As expected, mutation of this residue with an amino acid like Gln, having different structural and chemical properties, almost abrogates ADAMTS13 catalytic efficiency [44] (Fig. 4).

Asp235His and Ser263Cys Asp235 in the Lα4α6 loop follows the catalytic His234 and is highly conserved in the ADAMTS family (Fig. 2). Our model shows that Asp235 is shielded from the solvents and, rather surprisingly, its side chain points in the protein interior. Besides Asp235, other conserved polar amino acids nearby are buried in the protein structure (i.e., Ser263 and Ser266). Clearly, the burial of an uncompensated charge would be highly destabilizing [49]. However, the crystallographic structures of ADAMTS-1, -4, and -5 reveal that the buried Asp is hydrogen bonded with two conserved Ser/Thr residues, at positions equivalent to those occupied by Ser263 and Ser266 in M13, and with at least one buried structural water molecule. Perhaps, Asp → His mutation displaces the structural water molecule, likely present also in the M13 structure, but does not disrupt the hydrogen bond network linking Lα4α6 loop to the rest of the protein. This conclusion is consistent with clinical data showing that Asp235His exchange is associated with only mild clinical manifestation of TTP [45] (Fig. 4).

Similar considerations hold for the Ser263Cys substitution, at the beginning of the α6-helix, associated with mild clinical symptoms of TTP [43]. Our model predicts that this mutation does not perturb neither M13 structure nor function because the bulkier Cys-residue can be snugly accommodated at the mutation site.

Ala250Val Ala250 is located at the fourth position of the highly conserved Met-turn in the Lα4α6 loop, at the mouth of the S1′ site and preceding the structurally important Met249 [30] (Fig. 4 and Fig. 6F). Ala250Val mutation is predicted to dramatically decrease ADAMTS13 catalytic efficiency primarily by restricting accessibility of the S1′ site to substrate binding and secondarily by altering Met-turn conformation [46]. With respect to the latter point, the backbone geometry of the amino acid corresponding to Ala250 in ADAMTS-1, -4, and -5 (average dihedral angles: ϕ −59°±1, ψ +140°±5) is not compatible with the minimum energy conformation of Val (i.e., ϕ: −90°, ψ: +100°) [50] (Fig. 6F).

Arg268Pro Arg268 is located in the middle of α6-helix and helps to stabilize the active site conformation by forming a key salt bridge with Glu233, preceding the catalytic His234. Clearly, Arg → Pro exchange impairs salt-bridge formation and disrupts α6-helix, as expected form the known helix-breaking properties of proline [49]. These changes can dramatically alter the structure of the "lower" domain, contributing to the active-site, and easily explain how Arg268Pro mutation abrogates ADAMTS13 function [42,47] (Fig. 6G).

3.2.3. Effect of natural mutations on the energetics of M13 structure

The analysis reported above suggests that natural mutations found in TTP patients can variably destabilize the folded structure of M13, which therefore might undergo conformational transitions toward new, less active conformations. Even in the absence of gross structural changes, however, destabilization of the native state per se is expected to affect the energetics of enzyme catalysis [51].

Here, the effect of mutations on the conformational stability of the modeled M13 structure was estimated using the Fold-X empirical force field, a widely used program based on experimental free energy data [25]. The free energy of folding ($\Delta G = G_N - G_U$) is calculated between the structure of the native form and that of a hypothetical unfolded reference state for which no structural detail is available. For this reason, significant error is introduced in the Fold-X predictions of absolute ΔG values. Nevertheless, higher accuracy is achieved when the free energy difference is calculated between a mutant and the wild-type protein ($\Delta\Delta G = \Delta G^M - \Delta G^{WT}$). As expected, the data shown in Fig. 7 indicate that all mutations destabilize the folded M13 structure, compared to the wild-type enzyme, and that this relative destabilization favorably correlates with the decrease of proteolytic efficiency of M13 mutants and with the severity of TTP (see Table 1), in the sense that mutations associated with mild or moderate clinical manifestations of TTP have relative ΔΔG values lower than those mutations associated with severe TTP. For the amino acid exchanges D235H and S263C, Fold-X predicts a destabilization higher than that expected from the mild symptoms that the mutations cause in TTP patients. This apparent discrepancy can be explained

considering that, as discussed above, both substitutions might affect binding in the protein core of a buried water molecule, which is not taken into account in Fold-X calculations.

3.3. Modeling ADAMTS13-vWF interaction

3.3.1. Docking wild-type vWF(1604–1607) into M13 active site

The cleavable ^{1604}Val-Tyr-Met-Val^{1607} segment of vWF A2 domain, vWF(1604–1607), was manually docked into M13 binding cleft (Fig. 8). As already observed with metzincins and matrix metalloproteases (MMPs), the stereochemistry of the active site in the M13 model entails that peptidyl substrates bind in an extended conformation [28,29] (Fig. 2). This assumption is experimentally supported by the fact that (partial) unfolding of A2 domain is a prerequisite for ADAMTS13 cleavage [3,7]. β4-strand forms the upper rim of the active-site crevice and binds the peptide backbone in an antiparallel β-like structure (Fig. 8A), from left (N-terminal non-primed side) to right (C-terminal primed side), while the Lβ3β4 loop contributes to the CaBS-II and protrudes from the protein surface with a bulge-like structure, whose wide concave face shapes the S1 site. Similarly to other metzincins, substrate specificity is principally determined by the S1′ site, a deep hydrophobic cavity contributed by specific amino acids in the Lα4α6 loop (Val248-Pro256), in the N-terminal region of α4-helix (Val220, Thr221 and Ala223), and in the C-terminal end of α2-helix (Leu114), while the conserved Trp262 (Fig. 2) forms the hydrophobic floor of the cavity.

Docking was carried out using as a starting template the high-resolution structure of MMP12 bound to a peptidyl substrate derived from α1 collagen chain [26] (see Methods and Fig. S3). On the nonprimed side, Val1604 at P2 harbors Leu198 in the β4-strand and His228 in the catalytic site, while the carbonyl oxygen of Tyr1605 at P1 chelates the zinc ion (Fig. 8B). Of note, the aromatic side chain of Tyr1605 contacts the wide and accessible cavity of the S1 site on the protease surface. On the primed side, Met1606 at P1′ easily penetrates with its long side chain into the deep and apolar S1′ pocket, making numerous van der Waals contacts with Ala250 and Asp251 backbone atoms in the Lα4α6 loop, with Val220 and Thr221 in the α4-helix, and with His224 in the catalytic site (Fig. 8B). Notably, the polarizable Sγ of Met1606 contacts the aromatic ring of His224 in an energetically favorable interaction [48], that might contribute to strengthen vWF-ADAMTS13 complex. Finally, Val1607 at P2′ points toward the convex surface of the Lβ3β4 loop, shaping the S2′ site.

3.3.2. Docking vWF(1604–1607)/Met1606MetSO analog into M13 active site

The structure of M13 complexed to the peptide vWF(1604–1607) containing the substitution Met1606→MetSO, vWF(1604–1607)/Met1606MetSO, is shown in Fig. 9A. Although oxidation of Met to MetSO only slightly increases the side-chain volume by only 6–8 Å^3, it dramatically alters its physico-chemical properties in terms of hydrophobicity, polarizability and conformational propensity. Indeed, oxidation of Sγ converts a hydrophobic amino acid like Met (logP = 2.33) into a polar amino acid like MetSO (logP = −1.04) [52]. Hence, considering the apolar nature of the protease S1′ site and that of the vWF substrate segment ^{1599}QAPNLVY-MVTGNPA^{1612}, Met→MetSO exchange is expected to hinder productive binding of vWF to ADAMTS13 predominantly by weakening hydrophobic interactions. Next, the electrophilic Oδ-atom of MetSO abrogates the polarizable character of Met Sγ-atom [53], thus disrupting the stabilizing Met-His interaction previously highlighted. Finally, due to the tetrahedral geometry of Sγ-atom, Met oxidation produces a mixture of (R)- and (S)-MetSO diastereomers. The structure of M13-vWF complex clearly shows that the (R)-MetSO isomer

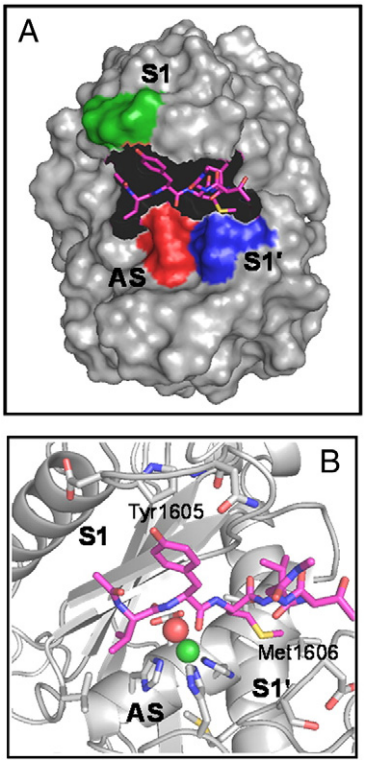

Fig. 8. M13–vWF interaction. (A) Docking of the vWF peptide ^{1604}Val-Tyr-Met-Val^{1607} into M13 active site. The protease surface is in gray; the regions comprising the S1 and S1′ site are colored green and blue, respectively, while the active site (AS) is in red. The ligand peptide is represented in stick (carbon, magenta; nitrogen, blue; oxygen, red; sulfur, yellow). (B) Close-up view of the interaction of the ligand peptide with M13 active site. The side chains of His224, His228, His234 and Glu225 in the active site are indicated; the zinc ion (green) and the catalytic water molecule (red) are also shown.

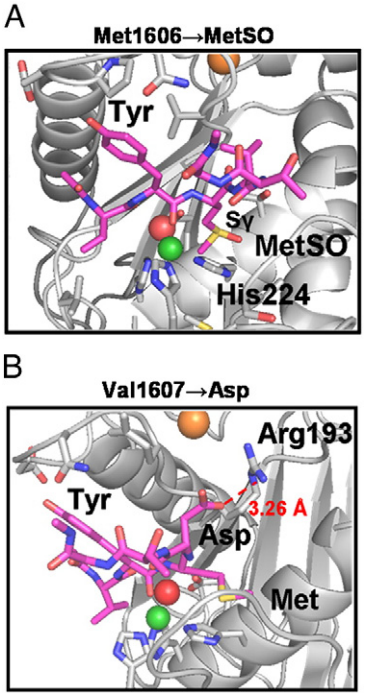

Fig. 9. Close-up view of the docking model of M13 with vWF(1604–1607) peptide segment, ^{1604}Val-Tyr-Met-Val^{1607}, containing the mutation Met1606MetSO (A) or Val1607Asp (B). Notably, the MetSO Oδ-atom clashes against the imidazole ring of His224 (panel A), while the negatively charged Asp-residue at position 1607 of vWF (panel B) harbors the positive Arg193 in the Lβ3β4 loop of M13, thus strengthening ADAMTS13–vWF interaction.

can be easily accommodated in the S1′ site, whereas the Oδ-atom of the (S)-MeSO isomer clashes against the imidazole ring of the catalytic His224 (Fig. 9A), thus hindering substrate binding to the proteases active site.

Analysis of M13-vWF interaction by the AMBER-99 force field [24] gives a difference in the free energy change of binding ($\Delta\Delta G_b = \Delta G_b^{Ox} - \Delta G_b^{WT}$) between the oxidized and unmodified vWF(1604–1607) of 2.0 kcal/mol, corresponding to a 30-fold decrease in the affinity for M13 at 25 °C. This value compares favorably with kinetic data showing that Met oxidation almost abrogates cleavage of VWF-74 [17,18] and that Met1606→Ala exchange reduces cleavage of VWF-115 by 15–18 fold [33].

3.3.3. Docking vWF(1604–1607)/Val1607Asp analog into M13 active site

Val1607Asp substitution at the substrate P2′ site has been identified as one of the key mutations of vWF in type 2A von Willebrand disease (T2A-VWD) [12,13], a common inherited human bleeding disorder characterized by loss UL-vWF polymers and hemorrhagic diathesis [12]. Notably, the recombinant Val1607Asp vWF mutant is cleaved by ADAMTS13 more efficiently than the wild-type protein [13]. Visual inspection of the A2 domain structure (3gxb) [54] reveals that Val1607 is buried in a hydrophobic environment, containing a structural water molecule that might favorably interact with Asp1607 in the vWF mutant. Our model (Fig. 9B) strongly suggests that, upon shear-induced unfolding of vWF A2 domain and exposure of the cleavable segment [3], Asp1607 can electrostatically couple with Arg193 nearby in the Lβ3β4 loop of the protease to form a stabilizing salt bridge, thus strengthening M13–vWF interaction and accelerating vWF hydrolysis.

4. Conclusions

Despite its key role in hemostasis and its involvement in different thrombotic or hemorrhagic diseases, the crystal structure of ADAMTS13 still awaits experimental determination, while only the structure of some non-proteolytic C-terminal domains is available [31]. Using homology modeling techniques, here we generated the structure of ADAMTS13 metalloprotease domain, M13. The final model was validated against all known mutations found in M13 sequence (Table 1), variably affecting proteolytic function and representing a natural protein engineering system useful for studying structure–activity relationships in ADAMTS13. In all cases, simple visual inspection of the model allowed us to easily explain the observed functional changes on the basis of the structural perturbation introduced upon mutation. Thereafter, we manually docked the vWF(1604–1607) peptide segment into the protease active site and demonstrated that the higher resistance of oxidized vWF to proteolysis by ADAMTS13 is mainly caused by a reduced binding affinity of the substrate, due to loss of hydrophobic and specific Met–His interactions as well as to steric hindrance introduced upon Met oxidation. Interestingly, our model also provided reasonable structural basis for explaining the hemorrhagic effect of vWF Val1607Asp mutation found in T2A-VWD. With respect to this point, our docking model may be also useful for designing (peptide-based) inhibitors with potential pharmacological applications in hemorrhagic diseases related to enhanced proteolysis of vWF by ADAMTS13 (e.g., T2A-VWD).

Acknowledgments

Financial support from MIUR (PRIN2007-grant:2007T9HTFB_002) to V.D.F. and R.D.C. (2007T9HTFB_003) is gratefully acknowledged. The atomic coordinates of M13-vWF(1604–1607) complex are available upon request to V.D.F.

Appendix A. Supplementary data

Supplementary data to this article can be found online at doi:10.1016/j.bpc.2011.07.007.

References

[1] D.D. Wagner, Cell biology of von Willebrand factor, Annu. Rev. Cell Biol. 6 (1990) 217–246.
[2] J.E. Sadler, von Willebrand factor assembly and secretion, J. Thromb. Haemost. Suppl. 1 (2009) 24–27.
[3] C. Baldauf, R. Schneppenheim, W. Stacklies, T. Obser, A. Pieconka, S. Schneppenheim, U. Budde, J. Zhou, F. Gräter, Shear-induced unfolding activates von Willebrand factor A2 domain for proteolysis, J. Thromb. Haemost. 7 (2009) 2096–2105.
[4] Z.M. Ruggeri, The role of von Willebrand factor in thrombus formation, Thromb. Res. Suppl. 1 (2007) S5–S9.
[5] X. Zhang, K. Halvorsen, C.Z. Zhang, W.P. Wong, T.A. Springer, Mechanoenzymatic cleavage of the ultralarge vascular protein von Willebrand factor, Science 324 (2009) 1330–1334.
[6] J.E. Sadler, von Willebrand factor: two sides of a coin, J. Thromb. Haemost. 3 (2005) 1702–1709.
[7] D.W. Chung, K. Fujikawa, Processing of von Willebrand factor by ADAMTS-13, Biochemistry 41 (2002) 11065–11070.
[8] M. Furlan, R. Robles, B. Lamie, Partial purification and characterization of a protease from human plasma cleaving von Willebrand factor to fragments produced by in vivo proteolysis, Blood 87 (1996) 4223–4234.
[9] P.J. Anderson, K. Kokame, J.E. Sadler, Zinc and calcium ions cooperatively modulate ADAMTS13 activity, J. Biol. Chem. 281 (2006) 850–857.
[10] N.A. Turner, L. Nolasco, Z.M. Ruggeri, J.L. Moake, Endothelial cell ADAMTS-13 and VWF: production, release, and VWF string cleavage, Blood 114 (2009) 5102–5111.
[11] L. Lotta, I. Garagiola, R. Palla, A. Cairo, F. Peyvandi, ADAMTS13 mutations and polymorphisms in congenital thrombotic thrombocytopenic purpura, Hum. Mutat. 31 (2010) 11–19.
[12] D. Ginsburg, B.A. Konkle, J.C. Gill, R.R. Montgomery, P.L. Bockenstedt, T.A. Johnson, A.Y. Yang, Molecular basis of human von Willebrand disease: analysis of platelet von Willebrand factor mRNA, Proc. Natl. Acad. Sci. U.S.A. 86 (1989) 3723–3727.
[13] W.A. Hassenpflug, U. Budde, T. Obser, D. Angerhaus, E. Drewke, S. Schneppenheim, R. Schneppenheim, Impact of mutations in the von Willebrand factor A2 domain on ADAMTS13-dependent proteolysis, Blood 107 (2006) 2339–2345.
[14] P. Pacher, J.S. Beckman, L. Liaudet, Nitric oxide and peroxynitrite in health and disease, Physiol. Rev. 87 (2007) 315–424.
[15] G. Ferrer-Sueta, R. Radi, Chemical biology of peroxynitrite: kinetics, diffusion, and radicals, ACS Chem. Biol. 4 (2009) 161–177.
[16] B. Alvarez, R. Radi, Peroxynitrite reactivity with amino acids and proteins, Amino Acids 25 (2003) 295–311.
[17] S. Lancellotti, V. De Filippis, N. Pozzi, F. Peyvandi, R. Palla, B. Rocca, S. Rutella, D. Pitocco, P. Mannucci, R. De Cristofaro, Formation of methionine sulfoxide by peroxynitrite at position 1606 of von Willebrand factor inhibits its cleavage by ADAMTS-13: a new prothrombotic mechanism in diseases associated with oxidative stress, Free Radic. Biol. Med. 48 (2010) 446–456.
[18] S. Lancellotti, V. De Filippis, N. Pozzi, L. Oggianu, S. Rutella, G.L. Scaglione, F. Maset, F. Payvandi, P.M. Mannucci, R. De Cristofaro, Oxidation of von Willebrand factor by polymorphonuclear cells accelerates its hydrolysis by leukocyte serine proteases: divergence from ADAMTS-13 proteolysis, J. Thromb. Haemost. 9 (2011) 1620–1627.
[19] M. Brownlee, Biochemistry and molecular cell biology of diabetic complications, Nature 414 (2001) 813–820.
[20] L. Mosyak, K. Georgiadis, T. Shane, K. Svenson, T. Hebert, T. McDonagh, et al., Crystal structures of the two major aggrecan degrading enzymes, ADAMTS4 and ADAMTS5, Protein Sci. 17 (2008) 16–21.
[21] M.D. Tortorella, A.G. Tomasselli, K.J. Mathis, M.E. Schnute, S.S. Woodard, G. Munie, et al., Structural and inhibition analysis reveals the mechanism of selectivity of a series of aggrecanase inhibitors, J. Biol. Chem. 284 (2009) 24185–24191.
[22] R.W. Hooft, G. Vriend, C. Sander, E.E. Abola, Errors in protein structures, Nature 381 (1996) 272.
[23] R.A. Laskowski, M.W. MacArthur, D.S. Moss, J.M. Thornton, PROCHECK: a program to check the stereochemical quality of protein structures, J. Appl. Cryst. 26 (1993) 283–291.
[24] J. Wang, P. Cieplak, P.A. Kollman, How well does a restrained electrostatic potential (RESP) model perform in calculating conformational energies of organic and biological molecules? J. Comput. Chem. 21 (2000) 1049–1074.
[25] R. Guerois, J.E. Nielsen, L. Serrano, Predicting changes in the stability of proteins and protein complexes: a study of more than 1000 mutations, J. Mol. Biol. 320 (2002) 369–387.
[26] I. Bertini, V. Calderone, M. Fragai, C. Luchinat, M. Maletta, K.J. Yeo, Snapshots of the reaction mechanism of matrix metalloproteinases, Angew. Chem. Int. Ed Engl. 45 (2006) 7952–7955.
[27] C. Lherbet, C. Gravel, J.W. Keillor, Synthesis of S-alkyl L-homocysteine analogues of glutathione and their kinetic studies with gamma-glutamyl transpeptidase, Bioorg. Med. Chem. Lett. 14 (2004) 3451–3455.
[28] W. Stöcker, W. Bode, Structural features of a superfamily of zinc-endopeptidases: the metzincins, Curr. Opin. Struct. Biol. 5 (1995) 383–390.

[29] F.X. Gomis-Rüth, Catalytic domain architecture of metzincin metalloproteases, J. Biol. Chem. 284 (2009) 15353–15357.
[30] A.E. Oberholzer, M. Bumann, T. Hege, S. Russo, U. Baumann, Metzincin's canonical methionine is responsible for the structural integrity of the zinc-binding site, Biol. Chem. 390 (2009) 875–881.
[31] M. Akiyama, S. Takeda, K. Kokame, J. Takagi, T. Miyata, Crystal structures of the noncatalytic domains of ADAMTS13 reveal multiple discontinuous exosites for von Willebrand factor, Proc. Natl. Acad. Sci. U.S.A. 106 (2009) 19274–19279.
[32] M.D. Gardner, C.K. Chion, R. de Groot, A. Shah, J.T. Crawley, D.A. Lane, A functional calcium-binding site in the metalloprotease domain of ADAMTS13, Blood 113 (2009) 1149–1157.
[33] R. de Groot, D.A. Lane, J.T. Crawley, The ADAMTS13 metalloprotease domain: roles of subsites in enzyme activity and specificity, Blood 116 (2010) 3064–3072.
[34] A. Veyradier, J.M. Lavergne, A.S. Ribba, B. Obert, C. Loirat, D. Meyer, J. Girma, Ten candidate ADAMTS13 mutations in six French families with congenital thrombotic thrombocytopenic purpura (Upshaw–Schulman syndrome), J. Thromb. Haemost. 2 (2004) 424–429.
[35] F. Peyvandi, S. Lavoretano, R. Palla, C. Valsecchi, G. Merati, R. De Cristofaro, E. Rossi, P.M. Mannucci, Mechanisms of the interaction between two ADAMTS13 gene mutations leading to severe deficiency of enzymatic activity, Hum. Mutat. 27 (2006) 330–336.
[36] R. Donadelli, F. Banterla, M. Galbusera, C. Capoferri, et al., In-vitro and in-vivo consequences of mutations in the von Willebrand factor cleaving protease ADAMTS13 in thrombotic thrombocytopenic purpura, Thromb. Haemost. 96 (2006) 454–464.
[37] G.G. Levy, W.C. Nichols, E.C. Lian, T. Foroud, J.N. McClintick, B.M. McGee, et al., Mutations in a member of the ADAMTS gene family cause thrombotic thrombocytopenic purpura, Nature 413 (2001) 488–494.
[38] S.C. Meyer, R. Jeddi, B. Meddeb, E. Gouider, B. Lämmle, J.A. Kremer Hovinga, A first case of congenital TTP on the African continent due to a new homozygous mutation in the catalytic domain of ADAMTS13, Ann. Hematol. 87 (2008) 663–666.
[39] H.B. Feys, I. Pareyn, R. Vancraenenbroeck, M. De Maeyer, H. Deckmyn, C. van Geet, K. Vanhoorelbeke, Mutation of the H-bond acceptor S119 in the ADAMTS13 metalloprotease domain reduces secretion and substrate turnover in a patient with congenital thrombotic thrombocytopenic purpura, Blood 114 (2009) 4749–4752.
[40] Y. Fujimura, M. Matsumoto, K. Kokame, A. Isonishi, K. Soejima, et al., Pregnancy-induced thrombocytopenia and TTP, and the risk of fetal death, in Upshaw–Schulman syndrome: a series of 15 pregnancies in 9 genotyped patients, Br. J. Haematol. 60 (2009) 1325–1332.
[41] M. Matsumoto, K. Kokame, K. Soejima, M. Miura, S. Hayashi, et al., Molecular characterization of ADAMTS13 gene mutations in Japanese patients with Upshaw–Schulman syndrome, Blood 103 (2004) 1305–1310.
[42] A. Hommais, J. Rayes, A. Houllier, B. Obert, P. Legendre, A. Veyradier, J.P. Girma, A.S. Ribba, Molecular characterization of four ADAMTS13 mutations responsible for congenital thrombotic thrombocytopenic purpura (Upshaw–Schulman syndrome), Thromb. Haemost. 98 (2007) 593–599.
[43] R. Schneppenheim, U. Budde, F. Oyen, D. Angerhaus, V. Aumann, et al., von Willebrand factor cleaving protease and ADAMTS13 mutations in childhood TTP, Blood 101 (2003) 1845–1850.
[44] Y. Shibagaki, M. Matsumoto, K. Kokame, S. Ohba, T. Miyata, Y. Fujimura, T. Fujita, Novel compound heterozygote mutations (H234Q/R1206X) of the ADAMTS13 gene in an adult patient with Upshaw–Schulman syndrome showing predominant episodes of repeated acute renal failure, Nephrol. Dial. Transplant. 21 (2006) 1289–1292.
[45] K. Assink, R. Schiphorst, S. Allford, D. Karpman, A. Etzioni, B. Brichard, N. van de Kar, L. Monnens, L. van den Heuvel, Mutation analysis and clinical implications of von Willebrand factor-cleaving protease deficiency, Kidney Int. 63 (2003) 1995–1999.
[46] T. Uchida, H. Wada, M. Mizutani, M. Iwashita, H. Ishihara, et al., Research Project on Genetics of Thrombosis: identification of novel mutations in ADAMTS13 in an adult patient with congenital thrombotic thrombocytopenic purpura, Blood 104 (2004) 2081–2083.
[47] K. Kokame, M. Matsumoto, K. Soejima, H. Yagi, H. Ishizashi, M. Funato, H. Tamai, M. Konno, K. Kamide, Y. Kawano, T. Miyata, Y. Fujimura, Mutations and common polymorphisms in ADAMTS13 gene responsible for von Willebrand factor cleaving protease activity, Proc. Natl. Acad. Sci. U.S.A. 99 (2002) 11902–11907.
[48] P. Chakrabarti, R. Bhattacharyya, Geometry of nonbonded interactions involving planar groups in proteins, Prog. Biophys. Mol. Biol. 95 (2007) 83–137.
[49] B.W. Matthews, Studies on protein stability with T4 lysozyme, Adv. Protein Chem. 46 (1995) 249–278.
[50] Y. Paterson, S.J. Leach, The effect of side-chain branching on the theoretically predicted conformational space available to amino acid residues, Macromolecules 11 (1978) 409–415.
[51] M.H. Olsson, W.W. Parson, A. Warshel, Dynamical contributions to enzyme catalysis: critical tests of a popular hypothesis, Chem. Rev. 106 (2006) 1737–1756.
[52] H.L. Schenck, G.P. Dado, S.H. Gellman, Redox-triggered secondary structure changes in the aggregated states of a designed methionine-rich peptide, J. Am. Chem. Soc. 118 (1996) 12487–12494.
[53] N. Brot, H. Weissbach, Biochemistry and physiological role of methionine sulfoxide residues in proteins, Arch. Biochem. Biophys. 223 (1983) 271–281.
[54] Q. Zhang, Y.F. Zhou, C.Z. Zhang, X. Zhang, C. Lu, T.A. Springer, Structural specializations of A2, a force-sensing domain in the ultralarge vascular protein von Willebrand factor, Proc. Natl. Acad. Sci. U.S.A. 106 (2009) 9226–9231.
[55] C. Tallant, A. Marrero, F.X. Gomis-Rüth, Matrix metalloproteinases: fold and function of their catalytic domains, Biochim. Biophys. Acta 1803 (2010) 20–28.